JPE 18-3-12

https://doi.org/10.6113/JPE.2018.18.3.766
ISSN(Print): 1598-2092 / ISSN(Online): 2093-4718

Modeling, Dynamic Analysis and Control Design of Full-Bridge LLC Resonant Converters with Sliding-Mode and PI Control Scheme

Kai Zheng†, Guodong Zhang*, Dongfang Zhou*, Jianbing Li*, and Shaofeng Yin*

†,*Zhengzhou Information Science and Technology Institute, Zhengzhou, China

Abstract

In this paper, a sliding mode and proportional plus integral (SM-PI) control combined with self-sustained phase shift modulation (SSPSM) for LLC resonant converters is presented. The proposed control scheme improves the transient response while preserving good steady-state performance. An averaged large signal model of an LLC converter with the ZVS modulation technique is developed for the SM control design. The sliding surface is obtained based on the input-output linearization concept. A system identification method is adopted to obtain the transform function of the LLC resonant converter, which is used to design the PI control. In order to reduce the inherent chattering problem in the steady state, the combined SM-PI control strategy is derived with fuzzy control, where the SM control is responsive during the transient state while the PI control prevails in the steady state. The combination of SSPSM and the SM-PI control provides ZVS operation, robustness and a fast transient response against step load variations. Simulation and experimental results validate the theoretical analysis and the attractive features of the proposed scheme.

Key words: LLC resonant converter, Phase shift modulation, Proportional plus integral control, Sliding mode control, Transient response, Zero voltage switching

I. INTRODUCTION

LLC resonant converters have been attracting more and more attention due to their inherent merits, including high efficiency, high power density, soft switching, and low EMI [1]-[4]. This topology has been extensively employed in industrial applications, such as renewable energy, electric vehicles, and the microwave transmitters of communication and radar systems. In some applications, the power converter encounters large signal disturbances including step load changes, large input-voltage changes, and large changes of the circuit parameters. For example, in microwave transmitter applications, the power converter load can change suddenly and repeatedly with the pulse modulation of the microwave transmitter. Considering these large signal disturbances, power converters should have a good transient response [5]-[8]. Although large signal disturbances exists in several applications, this paper focuses on the power converters used in pulse microwave transmitters.

Nowadays, proportional plus integral (PI) control is being widely applied to power converters, since they can realize local stability and good steady-state accuracy around the steady working point. However, PI control is not very effective in the presence of large signal variations [8]. Therefore, the nonlinear control approaches have drawn a lot of attention. The benefits of these approaches include improvements of the transient response, robustness, and stable behavior against parameter uncertainties. In the case of resonant converters, different nonlinear control methods have been reported such as fuzzy control [9], model predictive control [10], optimal control [11] and sliding mode (SM) control [12]-[15].

Sliding mode control is a special nonlinear control method with several advantages including a wide stability range, good dynamic response and strong robustness. There are several references on the SM control used in DC-DC resonant power converters [16]-[20]. In [16], SM control with strong robustness is used in LCC resonant power converters. In [17],

Manuscript received Jun. 5, 2017; accepted Jan. 6, 2018
Recommended for publication by Associate Editor Hao Ma.
†Corresponding Author: 401221515@qq.com
Tel: +86-186-2552-0283, Zhengzhou Information Sci. and Tech. Inst.
*Zhengzhou Information Science and Technology Institute, China

SM control is used in series resonant power converters, where the transient response is insensitive to load variations. In [18], SM control is used in CLL-T resonant power converters with discrete self-sustained oscillating modulation. In this case, input-output linearization control is adopted to design the sliding surface. Experimental results show that the proposed controller can provide robustness and a good transient response against load changes. In [19], [20], SM control is used in LLC resonant power converters with discrete pulse frequency modulation, which can significantly improve the system robustness and dynamic performance.

However, in these studies, the inherent chattering phenomenon of the SM control is not taken into consideration, which leads to a large output voltage ripple. In order to solve this chattering problem, some methods have been proposed, such as the boundary layer method, the equivalent control-based method, the observer-based method and the intelligent control method [8]. In addition, a combination of the sliding mode control and the proportional plus integral control (SM-PI) can also reduce the chattering phenomenon by using the SM control in the transient state and the PI control in the steady state [21], [22].

The major contribution of this paper is the design and development of a novel SM-PI control method, which depends on the application requirements of the LLC power converters used in microwave transmitters. A full-bridge LLC converter with the SM-PI control and self-sustained phase shift modulation (SSPSM) is demonstrated based on a DSP. Note that the zero voltage switching (ZVS) operation can be guaranteed by adopting SSPSM [23]-[25]. The dynamic model of the proposed LLC converter is built with the averaged large-signal modeling method. Then, the SM-PI control is proposed based on the dynamic model, and the fuzzy control is introduced to implement a smooth transition between the SM control and the PI control. The SM-PI control scheme can realize a good transient response and strong robustness from the SM control, and good stability can be obtained from the PI control.

The rest of this paper is organized as follows. The operating principle is discussed in Section II. After that, a large signal model of the LLC resonant converter is presented in Section III. Then, the SM-PI controller is designed in Section IV. Simulation and experimental results are given in Section V. Finally, some concluding remarks are provided in Section VI.

II. Description of the Proposed Full-Bridge LLC Converter

Fig. 1 shows a schematic of the proposed full-bridge LLC converter with a voltage multiplier rectifier. The switch pairs Q_1, Q_2, and Q_3, Q_4 form the full-bridge inverter. The resonant inductor L_r, the transformer magnetic inductor L_m and the resonant capacitor C_r form the LLC resonant tank. The diodes D_5, D_6 and the capacitors C_5, C_6 form the symmetrical multiplier rectifier. The SSPSM and SM-PI controls are adopted to implement the feedback control based on a DSP.

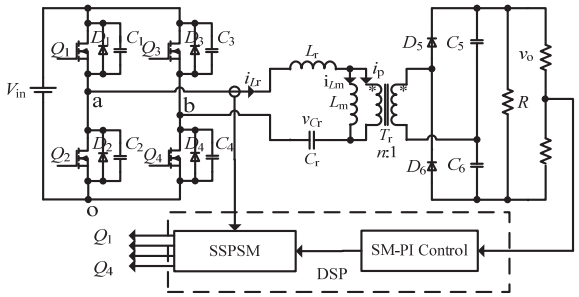

Fig. 1. Schematic of the proposed full-bridge LLC converter.

SSPSM is a special modulation method for resonant converters, which was inspired by the timing signal from the resonant current [23]-[25]. The modulation system is insensitive to parameter uncertainties, and the gate pulses of the switches can be changed adaptively according to the operating condition. When compared to the conventional frequency modulation (FM) control, the SSPSM has a much smaller frequency variation range, which makes it easy to optimize the magnetic components and to realize miniaturization. When compared to the conventional phase shift modulation (PSM) control, the SSPSM can realize a higher efficiency.

Fig. 2 shows the operating principle of the proposed full-bridge LLC converter with SSPSM. γ_a is the phase angle between the reverse resonant current $-i_{Lr}$ and the drain-source voltage v_{ao} of Q_2, and γ_b is the phase angle between the resonant current i_{Lr} and the drain-source voltage v_{bo} of Q_4. The sawtooth wave v_{st} is the modulation wave, whose amplitude V_p should be almost constant. v_{ca} and v_{cb} are the two modulation lines. v_{ca} is the upper modulation line, and v_{cb} is the lower modulation line, $v_{ca} \geq v_{cb}$. If the gradient k of v_{st} is assumed to be constant, v_{ca} and v_{cb} can be described by the following functions, $v_{ca} = k\gamma_a$, $v_{cb} = k\gamma_b$. Usually, v_{ca} is kept constant, and v_{cb} is used as a control variable to regulate the converter. If $v_{ca} < V_p$, the resonant current i_{Lr} lags the inverter output voltage v_{ab}, and ZVS can be implemented, which results in increased efficiency and improved reliability.

In general, the control angle γ_a is a continuous variable. In order to apply the SM control, a discrete SSPSM is proposed. In the discrete SSPSM, the control angle γ_b is changed between two fixed values ($\gamma_{b\text{-}max}$ and $\gamma_{b\text{-}min}$). Then, the proper control angle is determined by a new control variable u_{SM}. Then, the control angle γ_b is defined as:

$$\gamma_b = \gamma_{b\text{-}min} + (\gamma_{b\text{-}max} - \gamma_{b\text{-}min}) \cdot u_{SM} \tag{1}$$

$$u_{SM} = \begin{cases} 1 \\ 0 \end{cases} \tag{2}$$

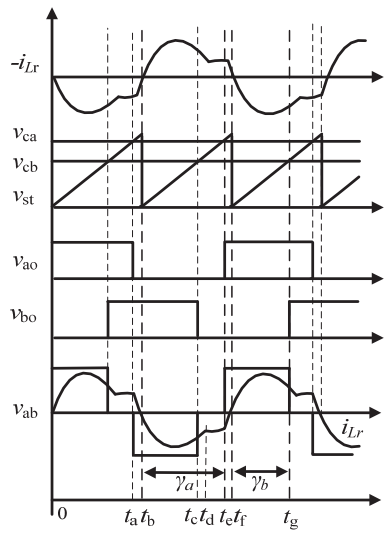

Fig. 2. Operating principle of the proposed full-bridge LLC converter with SSPSM.

III. Dynamic Modeling of the LLC Converter

The averaged large-signal modeling method is adopted to build a dynamic model. The detailed modeling method can be found in [26], [27]. Assuming ideal circuit components, the converter behavior can be represented by the following equations:

$$v_{Cr} + L_r \frac{di_{Lr}}{dt} + L_m \frac{di_{Lm}}{dt} = v_{ab} \tag{3}$$

$$C_r \frac{dv_{Cr}}{dt} = i_{Lr} \tag{4}$$

$$L_m \frac{di_{Lm}}{dt} = \mathrm{sgn}\left(i_{Lr} - i_{Lm}\right)\frac{nv_o}{2} \tag{5}$$

$$\frac{v_o}{R} + \frac{1}{2}C_o \frac{dv_o}{dt} = n \cdot abs\left(i_{Lr} - i_{Lm}\right) \tag{6}$$

where i_{Lr}, i_{Lm} and v_{Cr} are the resonant variables (resonant current, magnetizing current and resonant capacitor voltage), v_o is the output voltage, n is the transformer turns ratio, and C_o represents the same value as the filter capacitors C_5 and C_6.

The resonant variables i_{Lr}, i_{Lm} and v_{Cr} can be approximated by the fundamental harmonics as:

$$i_{Lr} = I_{Lr} \sin \omega_s t \tag{7}$$

$$v_{Cr} = V_{Cr} \sin\left(\omega_s t - \varphi_{Cr}\right) \tag{8}$$

$$i_{Lm} = I_{Lm} \sin\left(\omega_s t - \varphi_{Lm}\right) \tag{9}$$

The nonlinear terms v_{ab}, sgn(i_{Lr}–i_{Lm}) and abs(i_{Lr}–i_{Lm}) in (3)-(6), can be approximated with the fundamental components or the DC components [28], [29].

The inverter output voltage v_{ab} is also the input voltage of the LLC resonant tank. The frequency of v_{ab} is equal to the frequency of the LLC resonant variables. If v_{ab} is expanded to a Fourier series, only the fundamental component is the valuable excitation, and the other harmonics will be weakened by the resonant circuit.

$$\begin{aligned} v_{ab1\text{-}sin} &= \frac{4V_{in}}{\pi}\cos\frac{\gamma_a - \gamma_b}{2}\sin\left(\omega_s t + \pi - \gamma_a + \frac{\gamma_a - \gamma_b}{2}\right)\sin\omega_s t \\ &= -\frac{4V_{in}}{\pi}\cos\frac{\gamma_a - \gamma_b}{2}\sin\left(\omega_s t + \frac{\gamma_a - \gamma_b}{2} - \gamma_a\right)\sin\omega_s t \end{aligned} \tag{10}$$

The frequency of sgn(i_{Lr}–i_{Lm})nv_o/2 is equal to the resonant frequency, which can be approximately represented by the fundamental component. The fundamental component of sgn(i_{Lr}–i_{Lm}) can be described as:

$$[\mathrm{sgn}(i_{Lr} - i_{Lm})]_1 = \frac{4}{\pi}\frac{I_{Lr} - I_{Lm}\cos\varphi_{Lm}}{I_p}\sin\omega_s t + \frac{4}{\pi}\frac{I_{Lm}\sin\varphi_{Lm}}{I_p}\cos\omega_s t \tag{11}$$

where $I_p = \sqrt{{I_{Lr}}^2 + {I_{Lm}}^2 - 2I_{Lr}I_{Lm}\cos\varphi_{Lm}}$, $i_p = i_{Lr} - i_{Lm}$.

Only the DC component of abs(i_{Lr}–i_{Lm}) is the valuable excitation. The DC component of abs(i_{Lr}–i_{Lm}) can be described as:

$$\begin{aligned} [abs(i_{Lr} - i_{Lm})]_0 &= \frac{2}{\pi}\sqrt{(I_{Lr} - I_{Lm}\cos\varphi_{Lm})^2 + (I_{Lm}\sin\varphi_{Lm})^2} \\ &= \frac{2}{\pi}\sqrt{{I_{Lr}}^2 + {I_{Lm}}^2 - 2I_{Lr}I_{Lm}\cos\varphi_{Lm}} \end{aligned} \tag{12}$$

By substituting (7)-(12) into equations (3)-(6), based on the harmonic balance principle, the averaged large-signal model can be derived as:

$$L_r \frac{d\overline{i_{Lr}}}{dt} = -\frac{8V_{in}}{\pi^2}\frac{1}{2}(\cos\gamma_a + \cos\gamma_b) - \frac{8}{\pi^2}\frac{n\overline{v_o}}{2}\frac{\overline{i_{Lr}} - \overline{i_{Lm}}\cos\overline{\varphi_{Lm}}}{\overline{i_p}} - \overline{v_{Cr}}\cos\overline{\varphi_{Cr}} \tag{13}$$

$$C_r \frac{d\overline{v_{Cr}}}{dt} = \overline{i_{Lr}}\cos\overline{\varphi_{Cr}} \tag{14}$$

$$L_m \frac{d\overline{i_{Lm}}}{dt} = \frac{8}{\pi^2}\frac{n\overline{v_o}}{2}\frac{\overline{i_{Lr}}\cos\varphi_{Lm} - \overline{i_{Lm}}}{\overline{i_p}} \tag{15}$$

$$\frac{1}{2}C_o \frac{d\overline{v_o}}{dt} = n\overline{i_p} - \frac{\overline{v_o}}{R} \tag{16}$$

$$\frac{d\overline{\varphi_{Cr}}}{dt} = \omega_s - \frac{\overline{i_{Lr}}}{C_r \overline{v_{Cr}}}\sin\overline{\varphi_{Cr}} \tag{17}$$

$$\frac{d\overline{\varphi_{Lm}}}{dt} = \omega_s - \frac{8}{\pi^2}\frac{n\overline{v_o}}{2}\frac{1}{L_m}\frac{\overline{i_{Lr}}}{\overline{i_{Lm}}\,\overline{i_p}}\sin\overline{\varphi_{Lm}} \tag{18}$$

$$-\overline{v_{Cr}}\sin\overline{\varphi_{Cr}} + \overline{i_{Lr}}L_r\omega + n\overline{v_o}\frac{\overline{i_{Lm}}}{\overline{i_p}}\sin\overline{\varphi_{Lm}} = \frac{2}{\pi}V_{in}\left(\sin\gamma_a + \sin\gamma_b\right) \tag{19}$$

where the upper bar symbol denotes the averaged values.

IV. SM-PI Control Design

A. SM Control Design

Firstly, the relative degree of the controlled variable should be determined. The relative degree is defined as the smallest

derivative order of the output state variable with regard to time until the control variable appears explicitly. According to the control-oriented large-signal model, it can be shown that the relative degree is two. This is due to the fact that:

$$\frac{\partial}{\partial u_{\mathrm{SM}}}\left(\frac{d^{i}\overline{v_{\mathrm{o}}}}{dt^{i}}\right)=0 \qquad for \quad i=1 \tag{20}$$

$$\frac{\partial}{\partial u_{\mathrm{SM}}}\left(\frac{d^{i}\overline{v_{\mathrm{o}}}}{dt^{i}}\right)\neq 0 \qquad for \quad i=2 \tag{21}$$

In order to realize input-output linearization, the linear relationship between the input and output of the system should be obtained. In this sense, the desired closed-loop output voltage dynamic is imposed as a linear equation of the output voltage derivatives. The order of the output voltage dynamic should correspond with the relative degree. Then, the linear equation is expressed as:

$$a_2\frac{d^2\overline{v_{\mathrm{o}}}}{dt}+a_1\frac{d\overline{v_0}}{dt}+a_0(\overline{v_{\mathrm{o}}}-v_{\mathrm{ref}})=0 \tag{22}$$

Equation (22) can be further expressed as:

$$a_2\frac{d^2e_{vo}}{dt^2}+a_1\frac{de_{vo}}{dt}+a_0e_{vo}=0 \tag{23}$$

where $e_{\mathrm{vo}}=\overline{v_{\mathrm{o}}}-v_{\mathrm{ref}}$.

The sliding surface is found by combining the invariance condition $\dot{S}=0$. Then, the following equation is obtained as:

$$\dot{S}=a_2\frac{d^2e_{vo}}{dt^2}+a_1\frac{de_{vo}}{dt}+a_0e_{vo}=0 \tag{24}$$

By integrating (24), the sliding surface is derived as:

$$S=k_{\mathrm{p}}e_{vo}+k_{\mathrm{i}}\int e_{vo}dt+k_{\mathrm{d}}\frac{de_{vo}}{dt} \tag{25}$$

where $a_2=k_{\mathrm{d}}$, $a_1=k_p$ and $a_0=k_{\mathrm{i}}$. Equation (25) can be considered as an integral sliding mode surface, which has been widely analyzed in the PWM power converter [8], [30].

The equivalent control method is often used to design SM control systems. By applying the invariance condition and an averaged large signal model, the equivalent control signal can be obtained as:

$$\gamma_{\text{a-eq}}=\cos^{-1}\left[-\frac{\pi^2L_{\mathrm{r}}}{8V_{\mathrm{i}}\left(\overline{i_{Lr}}-\overline{i_{Lm}}\cos\overline{\phi_{Lm}}\right)}\left(\frac{C_{\mathrm{o}}\overline{i_{\mathrm{p}}}}{n}A-B\right)+C-\cos\gamma_{\mathrm{b}}\right] \tag{26}$$

where:

$$A=\left(\frac{4\mathrm{n}}{RC_{\mathrm{o}}{}^2}-\frac{2nk_{\mathrm{p}}}{C_{\mathrm{o}}k_{\mathrm{d}}}\right)\overline{i_{\mathrm{p}}}+\left(\frac{2k_{\mathrm{p}}}{RC_{\mathrm{o}}k_{\mathrm{d}}}-\frac{k_{\mathrm{i}}}{k_{\mathrm{d}}}-\frac{4}{R^2C_{\mathrm{o}}{}^2}\right)\overline{v_{\mathrm{o}}}+\frac{k_{\mathrm{i}}}{k_{\mathrm{d}}}v_{\mathrm{ref}}$$

$$B=2\overline{i_{Lm}}\frac{d\overline{i_{Lm}}}{dt}-2\overline{i_{Lr}}\frac{d\overline{i_{Lr}}}{dt}\cos\overline{\phi_{Lm}}+2\overline{i_{Lr}}\,\overline{i_{Lm}}\sin\overline{\phi_{Lm}}\frac{d\overline{\phi_{Lm}}}{dt}$$

$$C=-\frac{\pi^2}{4v_{\mathrm{i}}}\left(\frac{4n\overline{v_{\mathrm{o}}}}{\pi^2}\frac{\overline{i_{Lr}}-\overline{i_{Lm}}\cos\overline{\phi_{Lm}}}{\overline{i_{\mathrm{p}}}}-\overline{v_{Cr}}\cos\overline{\phi_{Cr}}\right)$$

The equivalent control law in (26) is complicated, and the phase variables ϕ_{Lm} and ϕ_{Cr} are difficult to obtain. Therefore, the equivalent control law is not practicable in resonant converters.

In this case, the switching function shown in (27) is obtained as the control law of the SM control. This is done by applying the reaching condition $S\cdot\dot{S}<0$. This control law is a bang-bang type control function. Its output is determined by the trajectory of the sliding surface.

$$u_{\mathrm{SM}}=\begin{cases}1 & for \quad S>0\\ 0 & for \quad S<0\end{cases} \tag{27}$$

Here, $S\cdot\dot{S}<0$ is the reaching condition, which can simultaneously meet the reaching condition and the existence condition of the sliding control.

When the sliding mode control is designed, the stability condition should be considered. In the sliding motion ($S=0$, $\dot{S}=0$), the ideal closed-loop dynamics can be expressed as:

$$k_d\frac{d^2e_{vo}}{dt^2}+k_p\frac{de_{vo}}{dt}+k_ie_{vo}=0 \tag{28}$$

The stability analysis is carried out using (28). Based on the Roth criterion, the output voltage asymptotically tends toward its reference signal if the following conditions are satisfied.

$$k_{\mathrm{i}}>0\,,\quad k_{\mathrm{p}}>0\,,\quad k_{\mathrm{d}}>0 \tag{29}$$

When selecting sliding mode coefficients, the coefficients must satisfy the stability condition, which can be inherently accomplished through the design of the sliding coefficients to meet the desired dynamical property.

Equation (28) can be rearranged into the standard second-order system form, which relates the sliding coefficients to the dynamic response of the converter during sliding mode operation.

$$\frac{d^2\overline{v}_{\mathrm{o}}}{dt^2}+\frac{k_{\mathrm{p}}}{k_{\mathrm{d}}}\frac{d\overline{v}_{\mathrm{o}}}{dt}+\frac{k_{\mathrm{i}}}{k_{\mathrm{d}}}\overline{v}_{\mathrm{o}}=\frac{k_{\mathrm{i}}}{k_{\mathrm{d}}}v_{\mathrm{ref}} \tag{30}$$

The relations can be expressed as functions of the bandwidth ω_0 and the damping ratio ξ.

$$\frac{k_{\mathrm{p}}}{k_{\mathrm{d}}}=2\xi\omega_0 \qquad \frac{k_{\mathrm{i}}}{k_{\mathrm{d}}}=\omega_0^2 \tag{31}$$

The design of the sliding mode coefficients can result in three possible types of responses: under-damped ($0\le\xi<1$), critically damped ($\xi=1$) and over-damped ($\xi>1$). In order to obtain a small voltage overshoot and a fast response time, an under-damped response is usually expected, where, ξ=0.707. $\omega_0=2\pi f_0$, f_0 is the expected frequency, where f_0 is designed to be one-tenth of the resonant frequency. Consequently, the design method of the sliding mode coefficients can be achieved. After selecting ξ, ω_0 and k_{d}, k_{p} and k_{i} can be calculated, where ξ=0.707, f_0=11.5K, $k_{\mathrm{d}}=2.25\times10^{-3}$, k_{p}=230 and $k_{\mathrm{i}}=1.17\times10^{7}$.

B. PI Control Design

While designing the PI control, it is necessary to get the transfer function of the full-bridge LLC resonant converter. Considering the complex circuit structure and operating modes of the LLC converter, it is difficult to obtain an accurate transfer function. In this paper, the system identification method is adopted to obtain the transfer function by analyzing PSpice simulation input and output data with the least square parameter estimation algorithm. In this system identification method, a complex converter is regarded as a black box, with only the input and output data for modeling, which can avoid the complicated analysis of the converter's working mechanism [31]-[33].

The simulation structure of the full-bridge LLC resonant converter is built with the PSpice simulation in Fig. 3. The main simulation parameters of the converter are shown in Table I. The converter can be treated as a black-box model structure, which is analyzed using the system identification method to fit the step response curve. Step response data can be collected with the simulation structure. The input and output data of this LLC simulation converter are sampled at the same time. Then, the least square parameter estimation algorithm is adopted to analyze the discrete data, and the least square estimation parameters can be obtained [31]-[33]. Based on the results of the parameter estimation, the discrete transfer function of the system is built as:

$$H(z)=\frac{b_1z^2+b_2z+b_3}{z^3-a_1z^2-a_2z-a_3}=\frac{9.708e7z^2-2.2e7z-4.479e7}{z^3-1.636z^2+0.5662z+0.07652} \quad (32)$$

The zero-order-hold method is used to convert the discrete transfer function $H(z)$ into a continuous transfer function $H(s)$.

$$H(s)=\frac{b_1's^3+b_2's^2+b_3's+b_4'}{s^4+a_1's^3+a_2's^2+a_3's+a_4'} =\frac{5.508e5s^3+6.664e10s^2+2.175e17s+4.777e21}{s^4+4.846e5s^3+1.64e11s^2+4.466e15s+1.07e19} \quad (33)$$

Fig. 4 shows a bode diagram of $H(s)$. As can be seen, the gain margin G_m is given as G_m=1.16dB, and the phase margin P_m is given as P_m=-1.5°, which does not satisfy the stability condition.

A PI regulator is adopted to perform serial correction, which can increase the system's phase margin and reduce the gain crossing frequency. The PI control law u_{PI} is shown as:

$$u_{PI}=k_{ps}S+k_{is}\int Sdt \quad (34)$$

where k_{ps} is the proportion coefficient, k_{is} is the integral coefficient, and S is the sliding surface. The system can become stable by adjusting k_{ps} and k_{is}. Then, the transfer function of the system can be expressed as:

$$H'(s)=H(s)G(s)=\frac{b_1's^3+b_2's^2+b_3's+b_4'}{s^4+a_1's^3+a_2's^2+a_3's+a_4'}\times(k_{ps}+\frac{k_{is}}{s}) \quad (35)$$

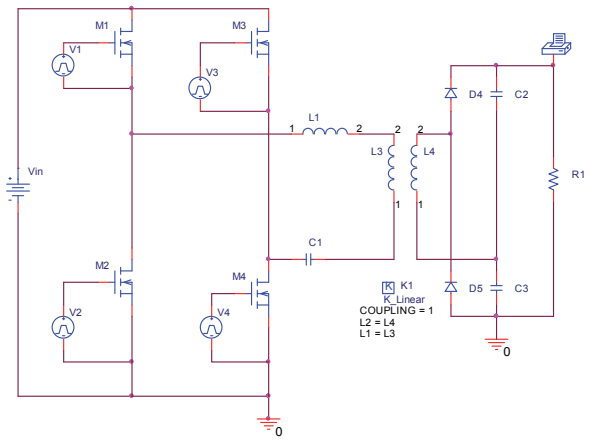

Fig. 3. PSpice simulation structure of a full-bridge LLC converter.

TABLE I
CONVERTER SIMULATION PARAMETERS

Input voltage (V_{in})	270 V
Resonant inductor (L_r)	64.6 μH
Resonant capacitor (C_r)	30 nF
Transformer magnetic inductor (L_m)	200 μH
Transformer turns ratio (n)	1:1
Output capacitor (C_o)	10 μF

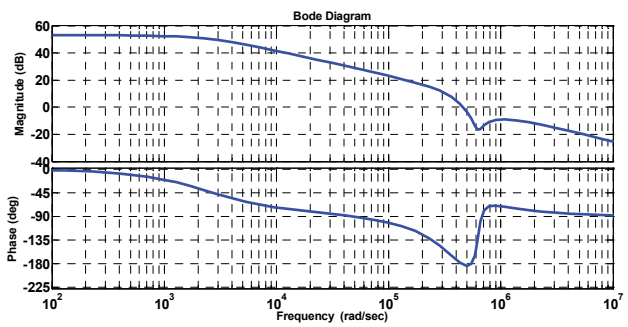

Fig. 4. Bode diagram of $H(s)$.

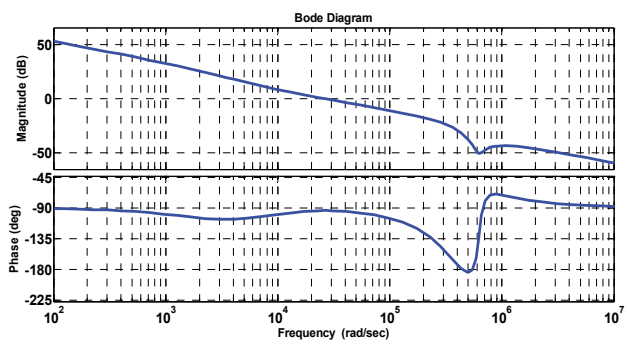

Fig. 5. Bode diagram of $H'(s)$.

Fig. 5 shows a bode diagram of $H'(s)$, where, k_{ps} is determined to be k_{ps}=0.02 and k_{is} is determined to be k_{is}=100. As can be seen, the crossing frequency is given as $\omega_c\approx$25kHz, the gain margin G_m is given as G_m=32dB, and the phase margin P_m is given as P_m=86°, which satisfy the stability condition.

C. SM-PI Control Design

The output voltage ripple is influenced by the inherent chattering phenomenon of the SM control. Consequently, the steady-state performance of the SM control is poor. In order to realize good control performance in the whole operating condition, the SM-PI control method is proposed by combining SM and PI controls, which can achieve a good transient response and strong robustness from the SM control, and good stability from the PI control. In the SM-PI control, the SM control is in charge of the transient response, and the PI control prevails in the steady state. Fuzzy logic control is introduced to implement a smooth transition between the sliding-mode control and the PI control [21], [22], [34].

Fig. 6 shows a fuzzy logic diagram of the SM-PI control, where, S is the sliding surface and the input of the fuzzy logic controller, SMALL and LARGE are defined to be member functions, and μ is the degree of the memberships. The whole control region is divided into different sub-regions with the parameters m_1 and m_2. When $S\in[-m_1, m_1]$, the PI control itself is in charge of the control. When $S\in[-\infty, -m_2]\cup[m_2, \infty]$, the SM control itself is in charge of the control. When $S\in[-m_2, -m_1]\cup[m_1, m_2]$, the PI control and SM control work in tandem through a fuzzy nonlinear switching function to produce a single controller output. The fuzzy parameters m_1 and m_2 are mainly related to the output voltage ripple and transient response time, which can be determined by fuzzy experiences including simulations and experiments. In order to implement a smooth transition between the SM and PI controls, a fuzzy member function should be designed. If a traditional linear function is adopted, the control law may vary very quickly around the switching point, and the transition between the SM and PI controls may not be smooth. Accordingly, a nonlinear function should be adopted. In this case, a radial basis function is applied, which can realize a smooth transition around the switching points of the PI and SM controls.

From the previous definition of the controller, it follows that the linguistic rules of the fuzzy logic supervisory controller should be defined as:

Rule 1: If S is SMALL, THEN $u=u_{\mathrm{PI}}$

Rule 2: If S is LARGE, THEN $u=u_{\mathrm{SMC}}$

where, u is the control output, u_{PI} is the PI control law, and u_{SMC} is the SM control law.

By applying the weighted sum defuzzification method, the overall output of the SM-PI control law $\mu_{\mathrm{SM\text{-}PI}}$ is given by:

$$u_{\mathrm{SM\text{-}PI}}=\frac{\sum_i \mu_i u_i}{\sum_i \mu_i}=k_{\mathrm{q}}u_{\mathrm{SM}}+(1-k_{\mathrm{q}})u_{\mathrm{PI}} \tag{36}$$

where, u_{i} is the control output of the rule i, and μ_{i} is the degree of membership for each rule i. In this case, the coefficient k_{q} can be represented as:

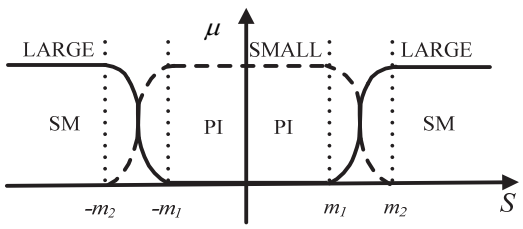

Fig. 6. Fuzzy logic diagram.

$$k_{\mathrm{q}}=\begin{cases}0, & |S|<m_1\\ \exp\left[-\dfrac{\left\|\,|S|-m_1\right\|^2}{2\sigma^2}\right], & m_1\le|S|\le m_2\\ 1, & |S|>m_2\end{cases} \tag{37}$$

where, the variable σ is related to the boundary variables m_1 and m_2, $\sigma=(m_2-m_1)/4$.

Note that the relationship between the SM-PI control law $u_{\mathrm{SM\text{-}PI}}$ and the SSPSM angle γ_{b} can be expressed as:

$$\gamma_{\mathrm{b}}=\gamma_{\mathrm{b\text{-}min}}+\left(\gamma_{\mathrm{b\text{-}max}}-\gamma_{\mathrm{b\text{-}min}}\right)\cdot u_{\mathrm{SM\text{-}PI}} \tag{38}$$

V. Simulation and Experimental Results

A. Simulation Results

In order to evaluate the performance of the proposed SM-PI control strategy, different simulation results have been presented in this section. These simulations were performed in MATLAB/SIMULINK simulator software. The main parameters of the designed converter are shown in Table II. Note that C_{o} represents the same value as the output filter capacitors C_5 /C_6.

Fig. 7(a) shows a simulation waveform of the output voltage with a traditional PI control in the presence of step load variations. Fig. 7(b) shows a simulation waveform of the output voltage with SM control in the presence of step load variations. Fig. 7(c) shows a simulation waveform of the output voltage with the SM-PI control in the presence of step load variations. The load resistance is changed between 500 Ω and 1000 Ω every 5 ms in the simulation. Obviously, it can be found that the SM-PI control has the best performance. The response time of the SM-PI control is faster, and the output voltage overshoot and undershoot of the SM-PI control are less than those of the PI control. The voltage ripple of the SM-PI control is less than that of the PI control in the steady-state.

Fig. 8 shows the SM-PI control law. As can be seen, the SM control is in charge of the transient response and the PI control prevails in the steady state. Accordingly, the SM-PI control avoids the inherent chattering problem of the SM control in the steady state and the poor dynamic performance of the PI control in the transient state.

TABLE II
CONVERTER PARAMETERS

Input voltage (V_{in})	270 V
Output voltage (V_o)	450 V
Resonant inductor (L_r)	64.6 μH
Resonant capacitor (C_r)	30 nF
Transformer magnetic inductor (L_m)	200 μH
Transformer turns ratio (n)	1:1
Output capacitor (C_o)	10 μF
Proportional gain (k_p)	230
Derivative gain (k_d)	2.25×10^{-3}
Integral gain (k_i)	1.17×10^{7}
Constant angle (γ_a)	170°
Maximum control angle ($\gamma_{b\text{-}max}$)	170°
Minimum control angle ($\gamma_{b\text{-}min}$)	90°
Lower boundary variable (m_1)	0.30
Upper boundary variable (m_2)	0.40

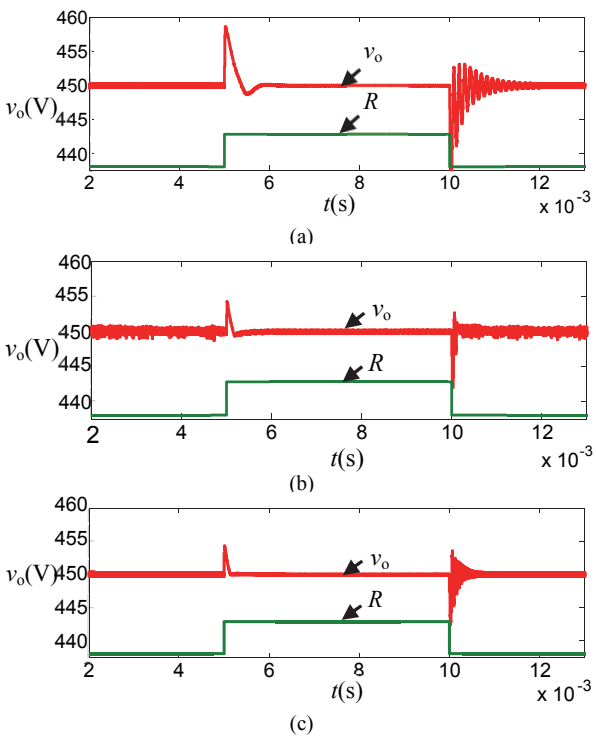

Fig. 7. Output-voltage simulation waveforms in the presence of step load variations. (a) PI controller. (b) SM controller. (c) SM-PI controller.

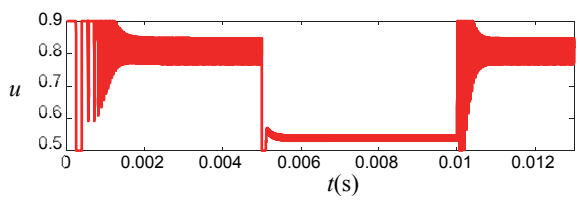

Fig. 8. SM-PI control law.

B. Experimental Results

In order to investigate the performance of the proposed control strategy, a laboratory prototype has been built, as shown in Fig. 9. The parameters of the converter are listed in Table II.

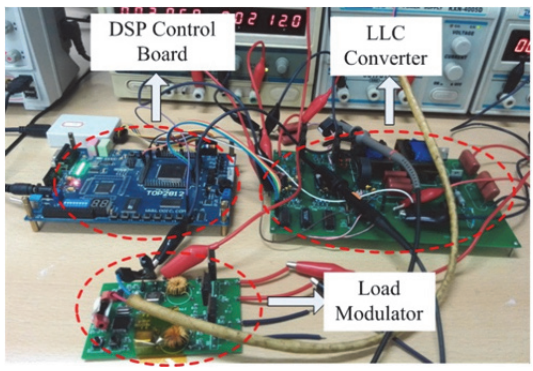

Fig. 9. Laboratory prototype.

1) Realization of a LLC Converter with the Proposed Control Scheme

Fig. 10(a) shows a block diagram of the LLC converter with SSPSM and the SM-PI control. A DSP board TMS320F2812 is used to implement the control scheme.

Fig. 10(b) shows a hardware schematic of an LLC converter with SSPSM. The general timer of the DSP event manager is set to the continuous incremental mode, and it is used to generate the sawtooth wave v_{st}. The comparison unit registers CMPR1 and CMPR2 separately to represent the modulation lines v_{ca} and v_{cb}. The logic signals v_{r1} and v_{r2} are obtained separately by comparing v_{st} with v_{ca} and v_{cb}. The zero-crossing moment of the resonant current can be captured by the DSP. Then, the signal v_{r3} can be easily generated. The logic signals v_{r1}, v_{r2} and v_{r3} can be converted into the drive signals LQ1–LQ4 through the logic operations of NOT gate, NAND gate and RS flip-flop. After that, the dead-time of LQ1-LQ4 is generated by the RCD circuit. Lastly, two drive chips Si8235 are used to drive the switches.

Fig. 10(c) shows the zero-crossing detection circuit. Zero-crossing capture is a vital part of the SSPSM design. If the zero-crossing moment cannot be correctly captured, SSPSM may not work. A hall-effect current sensor TBC06DS3.3 is adopted to sample the resonant current. In addition, the zero-crossing square-wave of the resonant current is obtained through an ultrafast comparator LT1720. However, the rising edge and falling edge of the square-wave may have some chattering. Therefore, the figuration function of this square-wave needs to be achieved through a RC filter and NOT gate 74LS14. In this way, the zero-crossing signal can be obtained in the correct manner, and sent to the capture port of the DSP.

Fig. 10(d) shows waveforms of the LLC converter with the proposed control scheme. The control law is converted to the input signal v_{cb} of the SSPSM. The sawtooth wave v_{st} is generated by the general timer of the DSP event manager. The logic signals v_{r1} and v_{r2} are obtained separately by comparing v_{st} with v_{ca} and v_{cb}. Then, the logic signal v_{r3} is generated by using the zero-crossing moment of the resonant current. After that, the three logic signals v_{r1}, v_{r2} and v_{r3} can be converted to the drive signals LQ1-LQ4 through the logic

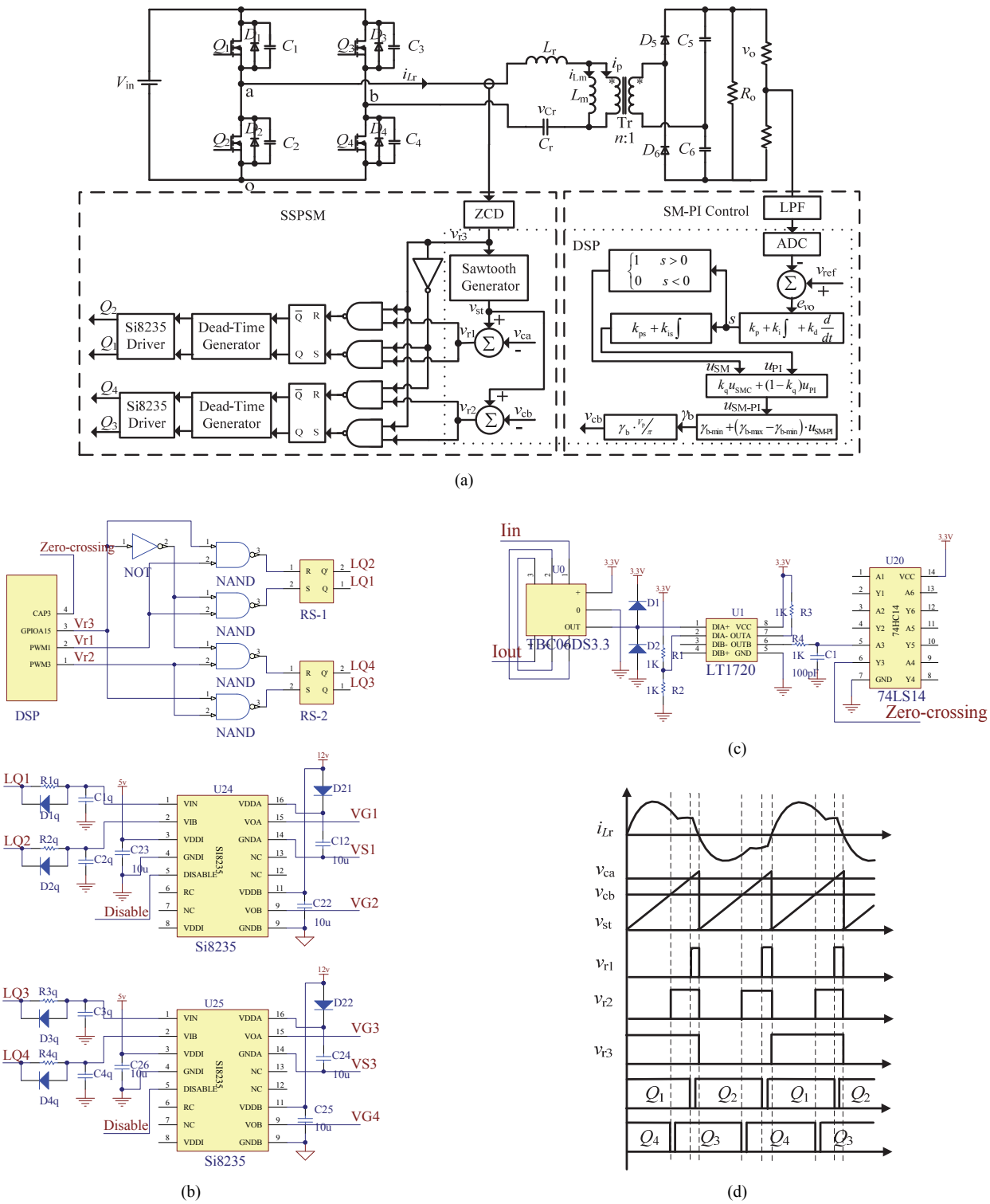

Fig. 10. LLC converter with SSPSM and the SM-PI control based on DSP. (a) Block diagram. (b) Hardware schematic. (c) Zero-crossing detection circuit. (d) Main waveforms.

operation of NOT gate, NAND gate and RS flip-flop. Lastly, the drive signals of the switches can be obtained through the dead-time generator circuit and the two drive chips Si8235.

In this paper, the SM-PI control is realized through a DSP, and the discretization process of the proposed method is expected.

Adopting the principle of the positional digital PID algorithm, the sliding surface $S = k_p e_{vo} + k_i \int e_{vo} dt + k_d \frac{de_{vo}}{dt}$ can be discretized as:

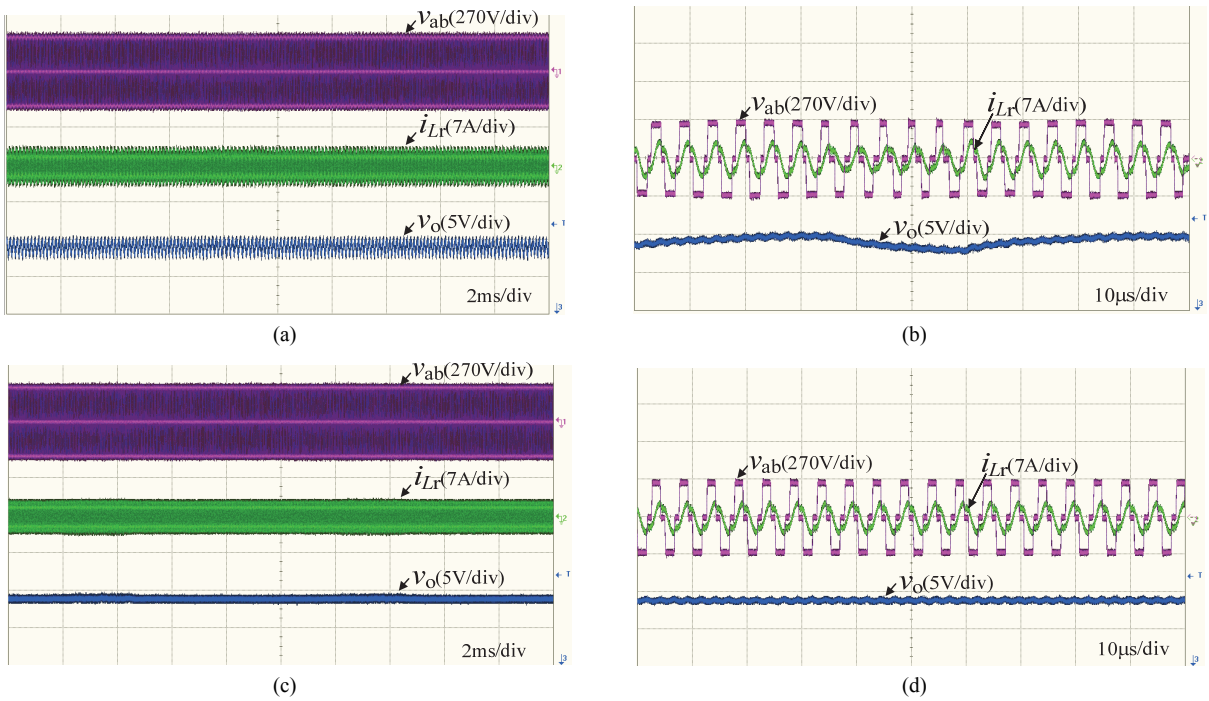

Fig. 11. Steady-state experimental waveforms. (a) SM controller. (b) SM controller. (c) SM-PI controller. (d) SM-PI controller.

$$S(n)=S(n-1)+k_{\mathrm{p}}\left[e_{vo}(n)-e_{vo}(n-1)\right]+k_{\mathrm{i}}Te_{vo}(n)+\frac{k_{\mathrm{d}}}{T}\left[e_{vo}(n)-2e_{vo}(n-1)+e_{vo}(n-2)\right] \quad (39)$$

In order to decrease the calculating time, function (39) can be simplified as:

$$S(n)=S(n-1)+a\cdot e_{vo}(n)+b\cdot e_{vo}(n-1)+c\cdot e_{vo}(n-2) \quad (40)$$

where $a=k_{\mathrm{p}}+k_{\mathrm{i}}T+\frac{k_{\mathrm{d}}}{T}$, $b=-(k_{\mathrm{p}}+\frac{2k_{\mathrm{d}}}{T})$, $c=\frac{k_{\mathrm{d}}}{T}$, T is the sampling time, $e_{vo}(n)$ is the output voltage error at the n time, $e_{vo}(n-1)$ is the output voltage error at the n-1 time, and $e_{vo}(n-2)$ is the output voltage error at the n-2 time.

Similarly, $u_{\mathrm{PI}}=k_{\mathrm{ps}}S+k_{\mathrm{is}}\int Sdt$ can be discretized as:

$$u_{\mathrm{PI}}(n)=u_{\mathrm{PI}}(n-1)+d\cdot S(n)+e\cdot S(n-1) \quad (41)$$

where $d=k_{\mathrm{ps}}+k_{\mathrm{is}}T$ and $e=-k_{\mathrm{ps}}$.

Analog-to-digital conversion occurs in each period of the sawtooth wave. The sampling period T can be approximately equal to half of a resonant period. Accordingly, the control gain parameters can be calculated as: $T=\frac{1}{2f_{\mathrm{r}}}=\frac{1}{2\times115000}\approx4.35\mu\mathrm{s}$, a=798, b=–1265, c=518, d=0.02 and e=–0.02.

2) Steady State Performance

Fig. 11 illustrates experimental waveforms of the resonant current i_{Lr}, inverter output voltage v_{ab}, and output voltage v_o with the SSPSM, where the load resistance is 1000 Ω. SSPSM can ensure that the resonant current i_{Lr} lags behind the inverter output voltage v_{ab} under any operating conditions to realize zero voltage switching (ZVS) of the switches by adjusting the shifting-phase angle, which results in an increased efficiency and improved reliability. As can be seen, since the zero-crossing points of the resonant current are used to generate the drive signals of the switches, i_{Lr} can always lag behind v_{ab}. In this situation, when one switch is turned on, the resonant current flows through the antiparallel body diode, the drain-source voltage is clamped to zero, and ZVS can be realized which reduces the switching losses. The experimental efficiency is 94%. Moreover, it can be found that the output voltage ripple with SM control is noticeably larger than that with the SM-PI control. In addition, note that the steady-state experimental waveforms of the PI controller are similar to those of the SM-PI controller.

3) Transient State Performance

Fig. 12 and Fig. 13 show the transient response in the presence of step load variations. A comparison is presented among the PI control, the SM control and the SM-PI control. On the one hand, the SM-PI controller is faster than the PI controller, and the SM-PI controller can provide less voltage overshoot and undershoot. On the other hand, the SM-PI controller can provide a noticeably lower steady-state output ripple than the SM controller. It can be found that the proposed SM-PI control scheme can realize good steady-state performance from the PI control and good transient-state performance from the SM control.

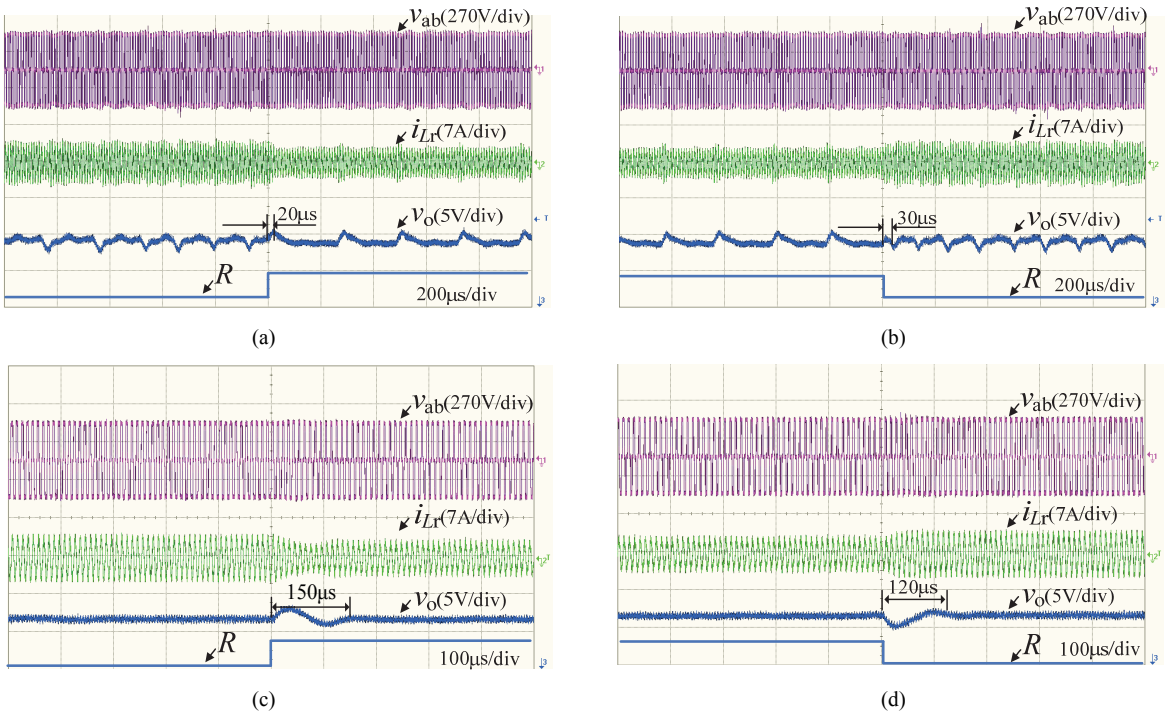

Fig. 12. Transient response with a SM controller and a PI controller in the presence of step load variations. (a) SM controller (from 500 Ω to 1000 Ω). (b) SM controller (from 1000 Ω to 500 Ω). (c) PI controller (from 500 Ω to 1000 Ω). (d) PI controller (from 1000 Ω to 500 Ω).

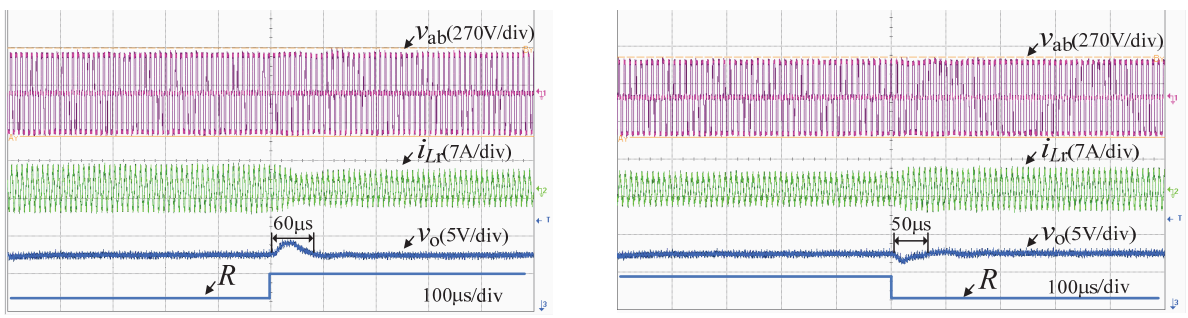

Fig. 13. Transient response with the SM-PI controller in the presence of step load variations. (a) SM-PI controller (from 500 Ω to 1000 Ω). (b) SM-PI controller (from 1000 Ω to 500 Ω).

VI. Conclusions

A SM-PI controller for full-bridge LLC converters is proposed in this paper. The SM controller is designed based on the large signal model of an LLC converter. The oriented-control model is derived for the converter under the SSPSM method, which guarantees ZVS operation. The sliding surface is obtained by using the input-output linearization concept. The PI control is designed based on a transfer function of an LLC converter, which is obtained with the system identification method. In order to address the chattering effect of the SM control, the SM-PI control is proposed by combining the SM control and the PI control. Fuzzy control is adopted to implement a smooth transition between the SM control and the PI control. Simulation and experimental results show that the SM-PI control can realize good steady-state and transient-state performance.

References

[1] H. Pan, C. He, and F. Ajmal, "Pulse-width modulation control strategy for high efficiency LLC resonant converter with light load applications," *IET Power Electron.*, Vol. 7, No. 11, pp. 2887-2894, Nov. 2014.

[2] C. Buccella, C. Cecati, H. Latafat, and P. Pape, "Observer-based control of LLC DC/DC resonant converter using extended describing functions," *IEEE Trans. Power Electron.*, Vol. 30, No. 10, pp. 5881-5891, Oct. 2015.

[3] X. Fang, H. Hu, J. Shen, and I. Batarseh, "Operation mode analysis and peak gain approximation of the LLC resonant converter," *IEEE Trans. Power Electron.*, Vol. 27, No. 4, pp. 1985-1995, Apr. 2012.

[4] Y. J. Park, H. J. Kim, J. Y. Chun, J. Y. Lee, Y. G. Pu, and K. Y. Lee, "A wide frequency range LLC resonant controller IC with a phase-domain resonance deviation prevention circuit for LED backlight units," *J. Power Electron.*, Vol. 15, No. 4, pp. 861-875, Jul. 2007.

[5] A. K. Singh, P. Das, and M. Pahlevaninezhad, "A novel high output voltage DC-DC LLC resonant converter with symmetric voltage quadrupler rectifier for RF communications," in *Proc. IEEE Telecommunications Energy Con- ference*, pp. 1-6, 2014.

[6] N. V. Bijeev, A. Malhotra, and V. Kumar, "Design and realization challenges of power supplies for space TWT," in *Proc. IEEE Vacuum Electronics Conference*, pp. 431-432, 2011.

[7] I. Barbi and R. Gules, "Isolated DC-DC converters with high-output voltage for TWTA Telecommunication Satellite Applications," *IEEE Trans. Power Electron.*, Vol. 18, No. 4, pp. 975-984, Apr. 2003.

[8] S. C. Tan, Y. M. Lai, and C. K. Tse, *Sliding Mode Control of Switching Power Converters Techniques and Implementation*, CRC Press, 2012.

[9] S. Selvaperumal, C.C.A. Rajan, and S. Muralidharan, "Stability and performance investigation of a fuzzy-controlled LCL resonant converter in an RTOS environment," *IEEE Trans. Power Electron.*, Vol. 28, No. 4, pp. 1817-1832, Apr. 2003.

[10] J. F. Hu and J. G. Zhu, "Multi-objective model-predictive control for high-power converters," *IEEE Trans. Energy Convers.*, Vol. 28, No. 3, pp. 652-663, Mar. 2013.

[11] H. Chen, E.K.K. Sng, and K.J. Tseng, "Optimum trajectory switching control for series parallel resonant converter," *IEEE Trans. Ind. Electron.*, Vol. 53, No. 5, pp. 1555-1563, May 2013.

[12] L. Shen, D. Lu, and C. Li, "Adaptive sliding mode control method for DC–DC converters," *IET Power Electron.*, Vol. 8, No. 9, pp. 1723-1732, Dec. 2013.

[13] J. Liu, F. Xiao, W. Ma, X. Fan, and W. Chen, "PWM-Based Sliding Mode Controller for Three-Level Full-Bridge DC-DC Converter that Eliminates Static Output Voltage Error," *Journal of Power Electron.*, Vol. 15, No. 2, pp. 378-388, Mar. 2015.

[14] I. Yazici, "Robust voltage-mode controller for DC–DC boost converter," *IET Power Electron.*, Vol. 8, No. 3, pp. 342-349, Mar. 2015.

[15] V. Enric, M.P. Adria, G. Germain, C.P. Angel, and M.S. Luis, "Discrete-time sliding-mode-based digital pulse width modulation control of a boost converter," *IET Power Electron.*, Vol. 8, No. 5, pp. 708-714, May 2015.

[16] M. Castilla, de Vicuña L. Garcia, J.M. Guerrero, J. Matas, and J. Miret, "Sliding-mode control of quantum series-parallel resonant converters via input–output linearization," *IEEE Trans. Ind. Electron.*, Vol. 52, No. 2, pp. 566-575, Feb. 2005.

[17] M. Castilla, de Vicuña L. Garcia, J. Matas, J. Miret, and J.C. Vasquez, "A comparative study of sliding-mode control schemes for quantum series resonant inverters," *IEEE Trans. Ind. Electron.*, Vol. 56, No. 9, pp. 3487-3495, Sep. 2009.

[18] J. L. Sosa, M. Castilla, J. Miret, de Vicuña, L. Garcia, and L. S. Moreno, "Sliding-mode input-output linearization controller for the DC/DC ZVS CLL-T resonant converter," *IEEE Trans. Ind. Electron.*, Vol. 59, No. 3, pp. 1554-1564, Mar. 2012.

[19] H. Ma, Q. W. Liu, and J. Guo, "A sliding-mode control scheme for LLC resonant DC/DC converter with fast transient response," *in Proc. IEEE Industrial Electronics Society Conference*, pp. 162-167, 2012.

[20] H. Ma, Q. W. Liu, and Y. X. Wang, "Discrete pulse frequency modulation control with sliding-mode implementation on LLC resonant DC/DC converter via input-output linearisation," *IET Power Electron.*, Vol. 7, No. 5, pp. 1033-1043, Sep. 2012.

[21] W. Wei, S. H. Xu, and X. C. Guo, "Method on hybrid sliding-mode variable structure control of induction motor," *Electric Machines and Control*, Vol. 13, No. 3, pp. 458-463, Mar. 2009.

[22] A. J. Abianeh, "Chattering-free classical variable structure direct torque controlled IPM synchronous motor drive by using PI Controller within boundary layer," in *Proc. IEEE Industrial Electronics and Applications,* pp. 65-656, 2011.

[23] Z. Y. Mohamed and K. J. Praveen, "A review and performance evaluation of control techniques in resonant converters," in *Proc. IEEE Industrial Electronics Society*, pp. 215-221, 2004.

[24] Z. Y. Mohamed, P. Humberto, and K. J. Praveen, "Self-sustained phase shift modulated resonant converters: modeling, design, and performance," *IEEE Trans. Power Electron.*, Vol. 21, No. 2, pp. 401-414, Feb. 2006.

[25] Z. Y. Mohamed, "Control and modeling of high frequency resonant DC/DC converters for powering the next generation microprocessors," PhD thesis, Queen's University, Kingston, 2005.

[26] M. Castilla, L. G. de Vicuña, M. Lopez, and V. Barcons, "An averaged large-signal modeling method for resonant converters," in *Proc. IEEE Industrial Electronics, Control and Instrumentation Conference*, pp. 215-221, 1997.

[27] M. Castilla, L. G. de Vicuña, O. Lopez, M. Lopez, and J. Matas, "Averaged large-signal model of quantum series-parallel resonant converter," *IEE Electronics Letters*, Vol. 35, No. 9, pp. 686-687, Apr. 1999.

[28] J. L. Sosa, M. Castilla, J. Miret, and L. G. de Vicuna, "Modeling and performance analysis of the DC/DC series–parallel resonant converter operating with discrete self-sustained phase-shift modulation technique," *IEEE Trans. Ind. Electron.*, Vol. 56, No. 3, pp. 697-705, Mar. 2009.

[29] C. Buccella, C. Cecati, H. Latafat, P. Pepe, and K. Razi, "Observer-based control of LLC DC/DC resonant converter using extended describing functions," *IEEE Trans. Power Electron.*, Vol. 30, No. 10, pp. 5881-5891, Oct. 2015.

[30] H. Li and X. Ye, "Sliding-Mode PID Control of DC-DC Converter," *in Proc. IEEE Industrial Electronics and Applications Conference*, pp. 730-734, 2010.

[31] W. P. Wang, Y. J. Shi, and D. B. Yang, "A new modeling method for the switching power converter," in *Proc. IEEE Power Electronics and Intelligent Transportation System,*

pp. 404-407, 2008.
[32] V. Valdivia and A. Barrado, "Black-box modeling of DC-DC converters based on transient response analysis and parametric identification methods," in *Proc. IEEE Applied Power Electronics Conference and Exposition,* pp. 1131-1138, 2010.
[33] V. Valdivia and A. Barrado, "Simple modeling and identification procedures for "black-box" behavioral modeling of power converters based on transient response analysis," *IEEE Trans. Power Electron.*, Vol. 24, No. 12, pp. 2776- 2790, Jul. 2009.
[34] J. Zhu, L. Wang, and F. Xue, "Fuzzy logic control by combining SMC and PI for PMSM," *Chinese Journal of Electric Drive*, Vol. 43, No. 7, pp. 43-48, Jul. 2013.

Kai Zheng was born in Henan Province, China. He received his B.S. and M.S. degrees in Electrical Engineering from the New Star Research Institute of Applied Technology, Hefei, China, in 2005 and 2009, respectively. He received his Ph.D. degrees in Electrical Engineering from the Zhengzhou Information Science and Technology Institute, Zhengzhou, China, in 2016. His current research interests include the modeling and control of resonant power converters.

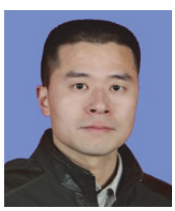

Guodong Zhang was born in Henan Province, China. He received his B.S. degree in Electrical Engineering from the Xi'an Communication Institute, Xi'an, China, in 2003; and his M.S. and Ph.D. degrees in Electrical Engineering from the Zhengzhou Information Science and Technology Institute, Zhengzhou, China, in 2008 and 2015, respectively. His current research interests include power electronics and control.

Dongfang Zhou was born in Zhejiang Province, China. He received his B.S. degree in Electrical Engineering from the Zhengzhou Information Science and Technology Institute, Zhengzhou, China, in 1983; his M.S. degree in Electrical Engineering from Xidian University, Xi'an, China, in 1989; and his Ph.D. degree in Electrical Engineering from Zhejiang University, Hangzhou, China, in 2005. He is presently working as a Professor at the Zhengzhou Information Science and Technology Institute. His current research interests include power electronics and control for microwave systems.

Jianbing Li was born in Hubei Province, China. He received his B.S., M.S. and Ph.D. degrees in Electrical Engineering from the Zhengzhou Information Science and Technology Institute, Zhengzhou, China, in 1999, 2002 and 2006, respectively. He is presently working as an Associate Professor at the Zhengzhou Information Science and Technology Institute. His current research interests include power electronics and control.

Shaofeng Yin was born in Henan Province, China. He received his B.S. and M.S. degrees in Electrical Engineering from the New Star Research Institute of Applied Technology, Hefei, China, in 2003 and 2007, respectively. His current research interests include the topology and control of power converters.